Volume 54 | Number 7 | 21 January 2018 | Pages 697–850

ChemComm

Chemical Communications

rsc.li/chemcomm

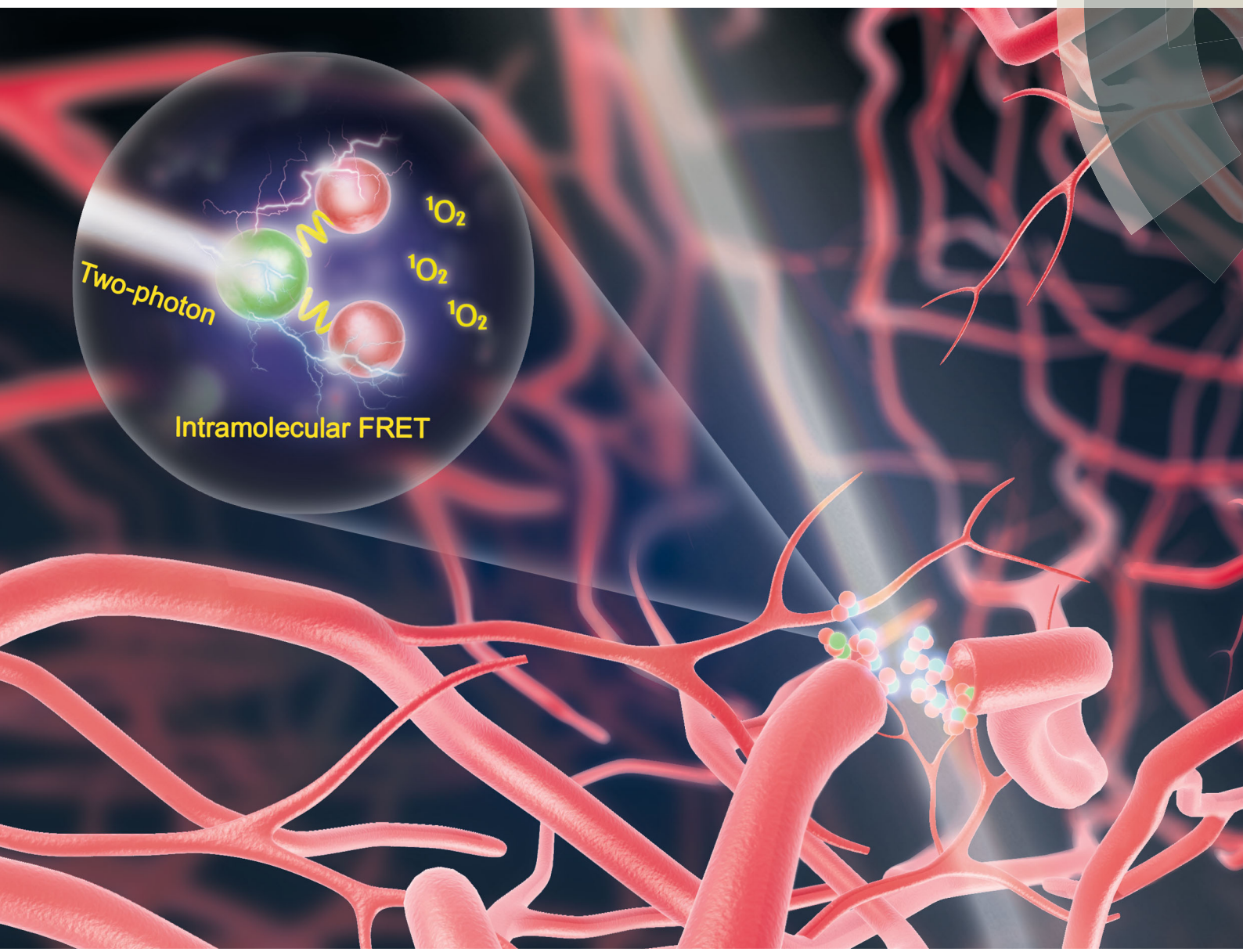

ISSN 1359-7345

ROYAL SOCIETY OF CHEMISTRY

COMMUNICATION

Yang Yang, Yanfei Qi, Jian Ru Gong *et al.*

Nitrogen-doped graphene quantum dots coupled with photosensitizers for one-/two-photon activated photodynamic therapy based on a FRET mechanism

ChemComm

COMMUNICATION

View Article Online
View Journal | View Issue

Cite this: *Chem. Commun.*, 2018, **54**, 715

Received 16th November 2017,
Accepted 29th November 2017

DOI: 10.1039/c7cc08820e

rsc.li/chemcomm

Nitrogen-doped graphene quantum dots coupled with photosensitizers for one-/two-photon activated photodynamic therapy based on a FRET mechanism†

Jiaheng Sun,[ab] Qi Xin,[b] Yang Yang,*[b] Hameed Shah,[b] Hongqian Cao,[ab] Yanfei Qi,*[a] Jian Ru Gong*[b] and Junbai Li[c]

A novel material with a large two-photon absorption cross-section was conjugated with a typical photosensitizer for inducing a FRET process. The photosensitizer can be excited by a one-/two-photon laser and then induced photo-toxicity *in vitro* and *in vivo*. The system presents great potential for improving treatment depth and the precision of traditional photodynamic therapy.

Two-photon photodynamic therapy (TP-PDT) is an emerging research field of recent years. As compared with traditional one-photon excitation, two-photon excitation has special advantages such as having high spatial resolution and strong penetrating capability. Therefore, two-photon techniques have been applied in PDT to improve its treatment depth and precision.[1–4] In the TP-PDT process, photosensitizers (PSs) absorb two photons of near-infrared light after two-photon laser excitation, allowing for deep tissue penetration and low photo-induced damage in tissue. So far, some novel two-photon PSs have been developed for TP-PDT.[5–15] However, most of them are special organic dyes which must be specially designed and synthesized through complex organic synthesis reactions. Furthermore, their limited two-photon absorption cross-section (TPAC) and low anti-bleaching abilities also hamper their use in practical TP-PDT applications. It is critical to develop a stable two-photon photosensitizer with a large TPAC and good biocompatibility.

In recent years, fluorescence resonance energy transfer (FRET) theory has been applied in the design of novel TP-PDT systems by some groups including ours.[16–21] In these systems, two-photon species and PSs, as energy donors and acceptors respectively, have been integrated together as one nano-system. After two-photon irradiation, PSs can be excited by two-photon species through FRET, which causes PSs to produce singlet oxygen and to kill cancer cells. In this way, traditional PSs can be endowed with a two-photon absorption function, which is a promising way to improve PDT treatment depth. In FRET induced TP-PDT systems, the two-photon material must have enough TPAC to ensure two-photon induced FRET efficiency. Recently, a series of nano-materials with such a two-photon absorption function have been reported for TP-PDT, such as semiconductor nanoparticles,[22] carbon nanomaterials,[23] silicon-based nanoparticles,[24] gold nanoparticles[25] and polymeric nanomaterials.[26] The emphasis is to select suitable species with a large TPAC, good biocompatibility and stability as donor materials to pair up with PSs in FRET induced TP-PDT systems.

In our previous work, we synthesized nitrogen-doped graphene quantum dots (N-GQDs). The materials exhibited a large TPAC (4.8×10^4 GM), good biocompatibility and extraordinary photo-stability, and could be applied in long-term two-photon fluorescence imaging of biological tissues.[27] In this work, a typical photosensitive drug, Rose Bengal (RB), was selected to pair up with N-GQD to induce the FRET process (Scheme 1). The two species were conjugated together to form N-GQD–RB through a simple coupling reaction. Therefore, RB can be excited by N-GQD under one- or two-photon laser irradiation and can then induce photo-toxicity through an intramolecular FRET process. Two-photon excitation endows N-GQD–RB with the feasibility

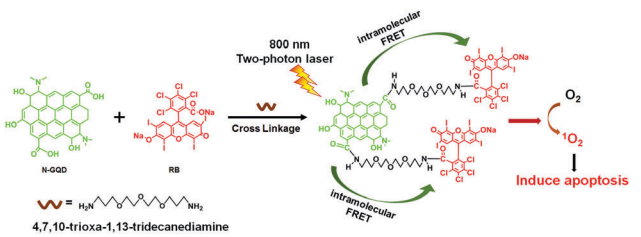

Scheme 1 Schematic illustration of the conjugation of N-GQD–RB and the application of TP-PDT *via* the FRET process.

[a] *School of Public Health, Jilin University, Changchun, China. E-mail: qiyanfei@jlu.edu.cn*
[b] *CAS Key Laboratory for Biomedical Effects of Nanomaterials and Nanosafety, National Center for Nanoscience and Technology, Beijing, China. E-mail: yangyang@nanoctr.cn, gongjr@nanoctr.cn*
[c] *CAS Key Laboratory of Colloid, Interface and Chemical Thermodynamics, Institute of Chemistry, Chinese Academy of Sciences, Beijing, China*

† Electronic supplementary information (ESI) available: Procedures for the synthesis and characterization used in this study and additional experimental information. See DOI: 10.1039/c7cc08820e

of deep tissue treatment and precise therapy. We investigated the intramolecular FRET mechanism of the coupling material and one-/two-photon induced photo-toxicity *in vitro* and *in vivo*. The system could hopefully be used to improve the depth and precision of traditional PDT.

In this system, N-GQD was conjugated to RB by 4,7,10-trioxa-1,13-tridecanediamine to synthesize N-GQD–RB. N-GQD was synthesized and characterized according to our previous work.[27] RB was selected as the energy acceptor because its maximum absorbance wavelength (560 nm) was close to the maximum emission wavelength (525 nm) of the energy donor (N-GQD). The large overlap region of the two spectra (Fig. 1a) indicated the possibility of FRET.[28] TEM images show that the diameters of N-GQD–RB are about 5 nm (Fig. 1c), a little larger than that of N-GQD (Fig. 1b), owing to the coupling of RB. The RB coupling was also identified using FT-IR spectroscopy, as shown in Fig. 1d. In comparison with the spectra of N-GQD and RB, the bands at 1292 (vibration of C–N), 1531 (vibration of N–H), and 1639 (vibration of C═O) cm^{-1} in the spectrum of N-GQD–RB were attributed to the amide bond.[29] In Fig. 1e and f, the CLSM images show that N-GQD and N-GQD–RB have good dispersion and high fluorescence intensity. The inset digital photograph images in Fig. 1e and f show that N-GQD has a strong green fluorescence under ultraviolet light irradiation, while the fluorescence after conjugation with RB is red. The UV/Vis spectrum of N-GQD–RB also displayed an increased absorption between 350 nm and 400 nm, and a red shift of the RB characteristic peak, which is attributed to the conjugation of N-GQD and RB (Fig. S1, ESI†).

The FRET between donors and acceptors results in the quenching of the donor fluorescence, decreasing of the donor fluorescence lifetime, and enhancement of the acceptor fluorescence lifetime. In light of this, a variety of methods to detect all of these processes have been reported.[30] In this study, the FRET process was confirmed through detecting the bleaching of the acceptor fluorescence, while simultaneously measuring the increase in donor fluorescence intensity. The acceptor dyes (RB) in a local region of N-GQD–RB were selected to be bleached with a high-intensity 559 nm laser, while ones beyond this region were not. As shown in Fig. S2 (ESI†), N-GQD–RB did not show the green fluorescence of the donor dye (N-GQD) before bleaching the RB, which confirmed that N-GQD transferred energy to RB. On the contrary, the region in which RB was bleached showed strong green fluorescence because there was no energy acceptor, which indicated that the FRET occurred between N-GQD and RB.[31]

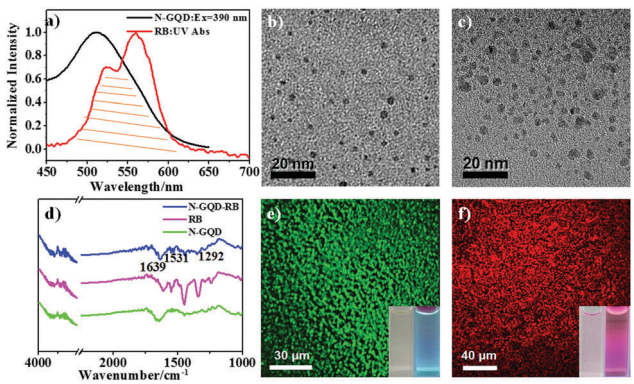

Fig. 1 Characteristics of N-GQD–RB. (a) Absorption spectrum of RB and emission spectrum of N-GQD. TEM images of (b) N-GQD and (c) N-GQD–RB. (d) FT-IR spectra of N-GQD, RB and N-GQD–RB. CLSM image of (e) N-GQD and (f) N-GQD–RB with excitation at 405 nm and 559 nm, respectively. Inset: Digital photograph of N-GQD and N-GQD–RB aqueous solution under the irradiation of daylight (left) and ultraviolet light (right).

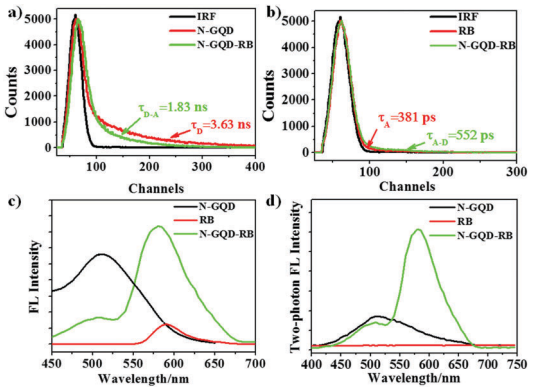

Fig. 2 Fluorescence decay curves of (a) N-GQD and N-GQD–RB (the fluorescence intensity was detected at 525 nm with excitation at 455 nm), and (b) RB and N-GQD–RB (the fluorescence intensity was detected at 580 nm with excitation at 455 nm). (c) Fluorescence spectra of N-GQD, RB and N-GQD–RB. The excitation wavelength was 405 nm. (d) Two-photon excitation fluorescence spectra of N-GQD, RB and N-GQD–RB. The excitation wavelength of the two-photon laser was 800 nm.

Time-resolved fluorescence measurements were used to confirm the efficiency of the FRET process. The fluorescence decay curves (Fig. 2a and b) were fitted with a bi-exponential fit. For N-GQD–RB, the average lifetime (τ_{D-A}) of the fluorescence decay at 525 nm was 1.83 nanoseconds (ns), which was shorter than that of N-GQD alone (τ_D = 3.63 ns). Moreover, the fluorescence decay of emission at 580 nm of RB had an average lifetime (τ_A) of 381 picoseconds (ps), but the average lifetime (τ_{A-D}) of the N-GQD–RB emission at 580 nm was extended to 552 ps. Both the shortened fluorescence lifetime of the donor and the lengthened fluorescence lifetime of the acceptor suggested that effective FRET occurs between N-GQD and RB.[32] The efficiency (E) of FRET was calculated by the equation:

$$E = (\tau_D - \tau_{D-A})/\tau_D$$

where τ_D and τ_{D-A} are the lifetimes of the donor before and after being linked with RB respectively. The efficiency of FRET was calculated to be 49.6% for this system.

The fluorescence spectra of N-GQD, RB and N-GQD–RB were obtained using a one-photon laser at 405 nm and a two-photon laser at 800 nm. As shown in Fig. 2d, RB (red spectrum) was hardly able to be excited by two-photon irradiation, which is because of the low TPAC of RB. However, the fluorescence intensity of N-GQD–RB (green spectrum) was greatly enhanced at 580 nm. Meanwhile, there was a decrease in the fluorescence intensity of N-GQD–RB at 520 nm compared with N-GQD alone, whether by one-photon or two-photon excitation (Fig. 2c and d).

These results also provide evidence that FRET happens between N-GQD and RB through one-/two-photon excitation.

Singlet oxygen is the main product during the photodynamic process. However, it is difficult to detect the level of singlet oxygen in physiological solution because of its short lifetime. Therefore, a selective singlet oxygen trap, ABDA (9,10-anthracenediylbis(methylene) dimalonic acid, a sensitive molecule to reactive oxygen species), was used to investigate the photogeneration of singlet oxygen from N-GQD, RB and N-GQD–RB, respectively. Measuring the decrease in absorption intensity of ABDA at 400 nm has been reported to allow the increase in the concentration of singlet oxygen in solution to be monitered.[33] As shown in Fig. 3a, during irradiation of the ABDA-containing N-GQD–RB solution using 480 nm light from a xenon lamp, the absorbance of ABDA at 400 nm decreased gradually with increased irradiation time. In Fig. 3b, the absorbance of ABDA decreased to 1.2% for N-GQD–RB after 40 minutes of irradiation and 57.9% for RB. However, the absorbance of ABDA with N-GQD and a blank sample (no N-GQD–RB) almost had no decrease under the same experimental conditions because of its inability to generate singlet oxygen (Fig. S3, ESI†). As a comparison, 530 nm light was also used to irradiate N-GQD–RB and RB at the same concentration. As shown in Fig. S4 (ESI†), the singlet oxygen yield was similar for N-GQD–RB and RB under this condition. This was attributed to N-GQD not being excited and failing to transfer energy to RB by 530 nm light irradiation. These results suggested that N-GQD–RB could enhance singlet oxygen generation based on intramolecular FRET.

The 3D reconstruction CLSM image was used to confirm the cellular uptake of N-GQD–RB after cancer cells (MCF-7) were co-cultured with N-GQD–RB for 4 hours. In Fig. 3c, the red dots are located outside of the nucleus and are surrounded by the cytomembrane of the cells, which meant that a large amount of N-GQD–RB had been internalized into the cytoplasm of cancer cells after incubation for 4 hours.

Furthermore, an MTT assay was applied to evaluate the cytotoxicity of N-GQD–RB. The photo-cytotoxicity was measured by irradiating MCF-7 cells for 10 minutes with a xenon lamp through a 480 nm filter after being co-cultured with N-GQD–RB for 4 hours. As shown in Fig. 3d, the cell viability exhibited a dose-dependent decrease, decreasing from 100% to 35% when the dose of N-GQD–RB increased from 0 to 60 μL, showing that N-GQD–RB is efficient for PDT *in vitro*. To compare the cytotoxicity of N-GQD–RB in the light and in the dark, we also tested the dark-cytotoxicity of N-GQD–RB co-cultured with cells in the dark for 24 hours with the same dose as that of the photo treatment group. In the dark treatment group, the cell viability remained above 80% even after exposure to a high concentration of N-GQD–RB, which suggested that N-GQD–RB had good biocompatibility and low dark toxicity for MCF-7 cells.

In addition, N-GQD–RB induced cytotoxicity by two-photon excitation was investigated by CLSM with a two-photon laser. The untreated MCF-7 cells (control) or cells treated with N-GQD, RB, or N-GQD–RB were irradiated with a two-photon laser at 800 nm, and then the dead cells were labeled by PI staining.[34] As shown in Fig. S5 (ESI†), the control group cells and the cells co-cultured with N-GQD or RB did not show any significant change in cell morphology after irradiation with a two-photon laser. However, there was a strong red fluorescence emission from cells treated with N-GQD–RB (Fig. 3e), and it can be seen that the cell morphology changes (Fig. 3f), which proved that N-GQD–RB induces strong two-photon toxicity. The results also verified that RB could be excited under two-photon laser irradiation through the FRET mechanism and induce two-photon cytotoxicity.

The coupled-material induced photo-toxicity also was investigated through *in vivo* experiment. The ears of mice were cleaned and then N-GQD–RB dispersed solution was injected into the mouse *via* the tail vein. Fig. S6a and b (ESI†) show the two-photon and one-photon images of the same blood vessels at different vertical depths. The fluorescence intensity decreases with the increase of depth, which is mainly because of the scattering of excited fluorescence. However, obviously, deeper blood vessels were observed with two-photon excitation. The blood vessels in the two-photon images were much clearer and had a higher signal-to-noise ratio than those in the one-photon images. These results show a great potential of N-GQD–RB for application in precise and deep therapy after two-photon excitation. Then, an artery was selected to perform the blood vessel closure experiment. As shown in Fig. 4a, the blood vessel in the scanned area shows no fluorescent signal after irradiation for about 8 minutes, which indicates the closure of the blood vessel. The control group was tested with the same dose of FITC-dextran and given the same dose of irradiation. However, the images (Fig. 4b) show no significant change after irradiation. These results exclude the interference of the laser irradiation itself. The effect benefits from high spatial selectivity and strong penetrating capability of two-photon excitation. We believe this technology is extremely helpful for some delicate operations, such as in the eye or brain, which is unattainable by conventional one-photon PDT.

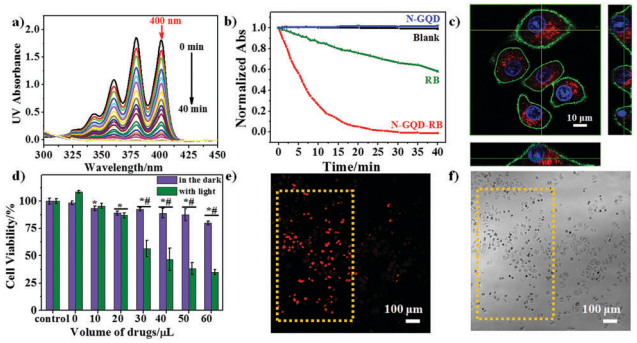

Fig. 3 (a) Absorption spectra of ABDA in the presence of N-GQD–RB under irradiation for different periods of times. (b) Normalized absorbance changes of ABDA caused by singlet oxygen oxidation plotted against irradiation time at 400 nm with different drugs (irradiation at 480 nm). (c) The 3D reconstruction CLSM image of MCF-7 cells co-cultured with N-GQD–RB for 4 hours; the orthogonal section images at the bottom and on the right were recorded along the yellow lines. (d) Cell viability of MCF-7 cells cultured under various conditions. $*p < 0.05$ for cells with different N-GQD–RB doses *vs.* control. $\#p < 0.05$ for cells with the same N-GQD–RB dose after light treatment *vs.* no light treatment. (e) The CLSM images of MCF-7 cells co-cultured with N-GQD–RB, and stained with PI. (f) Transmission light images of MCF-7 cells.

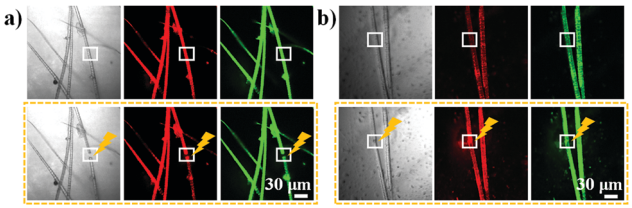

Fig. 4 Pre-irradiation and post-irradiation images of the ear blood vessels of mice treated with (a) N-GQD–RB or (b) FITC-dextran, and two-photon excitation. Ex: 800 nm. Em: 575–630 nm (the middle image); 495–540 nm (the right image).

In summary, we have synthesized stable photosensitizer-coupled graphene quantum dots, N-GQD–RB, which can be used for two-photon-induced PDT based on the FRET mechanism. Nitrogen-doped graphene quantum dots (N-GQD) with a large TPAC, as two-photon donors, were conjugated with traditional photosensitizers RB, as acceptors. The experimental results suggest that the materials possess good photo-stability and biocompatibility. RB can be excited by N-GQD with a one- or two-photon laser through an intramolecular FRET process. N-GQD–RB exhibits high cytotoxicity after irradiation under one- or two-photon laser irradiation. Furthermore, two-photon induced PDT was also verified through blocking the targeted blood vessel with high precision utilizing only a very small amount of the drug and a low dose of two-photon irradiation. Therefore, N-GQD–RB exhibits a high potential in one- or two-photon PDT for improving treatment depth and precision.

We are thankful to the National Nature Science Foundation of China (21673056, 21433010, 21320102004 and 81402719) for financial support. Yanfei Qi is particularly thankful to the Norman Bethune Program of Jilin University (2015228) for financial assistance. Jian Ru Gong particularly thanks the financial support from National Key R&D Program "nanotechnology" special focus (2016YFA0201600).

Conflicts of interest

The authors declare no conflicts of interest.

Notes and references

1 M. Triesscheijn, P. Baas, J. H. M. Schellens and F. A. Stewart, *Oncologist*, 2006, **11**, 1034–1044.
2 M. Pawlicki, H. A. Collins, R. G. Denning and H. L. Anderson, *Angew. Chem., Int. Ed.*, 2009, **48**, 3244–3266.
3 Y. Z. Shen, A. J. Shuhendler, D. J. Ye, J. J. Xu and H. Y. Chen, *Chem. Soc. Rev.*, 2016, **45**, 6725–6741.
4 Y. Zhang, T.-T. Shen, A. M. Kirillov, W.-S. Liu and Y. Tang, *Chem. Commun.*, 2016, **52**, 7939–7942.
5 C. Rouxel, M. Charlot, Y. Mir, C. Frochot, O. Mongin and M. Blanchard-Desce, *New J. Chem.*, 2011, **35**, 1771–1780.
6 Y. C. Zheng, M. L. Zheng, K. Li, S. Chen, Z. S. Zhao, X. S. Wang and X. M. Duan, *RSC Adv.*, 2015, **5**, 770–774.
7 B. Gu, W. Wu, G. Xu, G. Feng, F. Yin, P. H. J. Chong, J. Qu, K.-T. Yong and B. Liu, *Adv. Mater.*, 2017, DOI: 10.1002/adma.201701076.
8 N. Alifu, X. Dong, D. Li, X. Sun, A. Zebibula, D. Zhang, G. Zhang and J. Qian, *Mater. Chem. Front.*, 2017, **1**, 1746–1753.
9 L. Guo, J. Ge, Q. Jia, H. Zhang, W. Liu, G. Niu, S. Liu, J. Gong, S. Hackbarth and P. Wang, *Adv. Healthcare Mater.*, 2017, DOI: 10.1002/adhm.201601431.
10 J. L. Geng, K. Li, D. Ding, X. H. Zhang, W. Qin, J. Z. Liu, B. Z. Tang and B. Liu, *Small*, 2012, **8**, 3655–3663.
11 Q. Zou, H. Zhao, Y. Zhao, Y. Fang, D. Chen, J. Ren, X. Wang, Y. Wang, Y. Gu and F. Wu, *J. Med. Chem.*, 2015, **58**, 7949–7958.
12 J. Pille, S. A. van Lith, J. C. van Hest and W. P. Leenders, *Biomacromolecules*, 2017, **18**, 1302–1310.
13 Q. Zou, M. Abbas, L. Zhao, S. Li, G. Shen and X. Yan, *J. Am. Chem. Soc.*, 2017, **139**, 1921–1927.
14 N. Zhang, F. Zhao, Q. Zou, Y. Li, G. Ma and X. Yan, *Small*, 2016, **12**, 5936–5943.
15 K. Liu, R. Xing, Q. Zou, G. Ma, H. Möhwald and X. Yan, *Angew. Chem., Int. Ed.*, 2016, **55**, 3036–3039.
16 S. Kim, T. Y. Ohulchanskyy, H. E. Pudavar, R. K. Pandey and P. N. Prasad, *J. Am. Chem. Soc.*, 2007, **129**, 2669–2675.
17 I. Roy, T. Y. Ohulchanskyy, D. J. Bharali, H. E. Pudavar, R. A. Mistretta, N. Kaur and P. N. Prasad, *Proc. Natl. Acad. Sci. U. S. A.*, 2005, **102**, 279–284.
18 S. H. Cheng, C. C. Hsieh, N. T. Chen, C. H. Chu, C. M. Huang, P. T. Chou, F. G. Tseng, C. S. Yang, C. Y. Mou and L. W. Lo, *Nano Today*, 2011, **6**, 552–563.
19 H. L. Liu, Y. Yang, A. H. Wang, M. J. Han, W. Cui and J. B. Li, *Adv. Funct. Mater.*, 2016, **26**, 2561–2570.
20 B. Sun, L. Wang, Q. Li, P. He, H. Liu, H. Wang, Y. Yang and J. Li, *Biomacromolecules*, 2017, **18**, 3506–3513.
21 Y. Yang, H. Liu, M. Han, B. Sun and J. Li, *Angew. Chem.*, 2016, **55**, 13538–13543.
22 S. Dayal and C. Burda, *J. Am. Chem. Soc.*, 2008, **130**, 2890–2891.
23 C. Fowley, N. Nomikou, A. P. McHale, B. McCaughan and J. F. Callan, *Chem. Commun.*, 2013, **49**, 8934–8936.
24 E. Secret, M. Maynadier, A. Gallud, A. Chaix, E. Bouffard, M. Gary-Bobo, N. Marcotte, O. Mongin, K. El Cheikh, V. Hugues, M. Auffan, C. Frochot, A. Morere, P. Maillard, M. Blanchard-Desce, M. J. Sailor, M. Garcia, J. O. Durand and F. Cunin, *Adv. Mater.*, 2014, **26**, 7643–7648.
25 T. T. Zhao, K. Yu, L. Li, T. S. Zhang, Z. P. Guan, N. Y. Gao, P. Y. Yuan, S. Li, S. Q. Yao, Q. H. Xu and G. Q. Xu, *ACS Appl. Mater. Interfaces*, 2014, **6**, 2700–2708.
26 X. Q. Shen, F. He, J. H. Wu, G. Q. Xu, S. Q. Yao and Q. H. Xu, *Langmuir*, 2011, **27**, 1739–1744.
27 Q. Liu, B. D. Guo, Z. Y. Rao, B. H. Zhang and J. R. Gong, *Nano Lett.*, 2013, **13**, 2436–2441.
28 K. E. Sapsford, L. Berti and I. L. Medintz, *Angew. Chem., Int. Ed.*, 2006, **45**, 4562–4588.
29 B. K. Singh, R. K. Sharma and B. S. Garg, *Spectrochim. Acta, Part A*, 2006, **63**, 96–102.
30 A. K. Kenworthy, *Methods*, 2001, **24**, 289–296.
31 J. B. Dictenberg, W. Zimmerman, C. A. Sparks, A. Young, C. Vidair, Y. X. Zheng, W. Carrington, F. S. Fay and S. J. Doxsey, *J. Cell Biol.*, 1998, **141**, 163–174.
32 J. P. Lai, B. P. Shah, E. Garfunkel and K. B. Lee, *ACS Nano*, 2013, **7**, 2741–2750.
33 I. Roy, T. Y. Ohulchanskyy, H. E. Pudavar, E. J. Bergey, A. R. Oseroff, J. Morgan, T. J. Dougherty and P. N. Prasad, *J. Am. Chem. Soc.*, 2003, **125**, 7860–7865.
34 H. Lecoeur, *Exp. Cell Res.*, 2002, **277**, 1–14.

